Effects of Crystallographic Anistropy on Orthogonal Micromachining of Single-Crystal Aluminum

Benjamin L. Lawson

Nithyanand Kota

O. Burak Ozdoganlar[1]
e-mail: ozdoganlar@cmu.edu

Department of Mechanical Engineering,
Carnegie Mellon University,
Pittsburgh, PA 15213

Anisotropy of workpiece crystals has a significant effect in micromachining since the uncut chip thickness values used in micromachining are commensurate with characteristic dimensions of crystals in crystalline materials. This paper presents an experimental investigation on orthogonal micromachining of single-crystal aluminum at different crystallographic orientations for varying uncut chip thicknesses and cutting speeds using a diamond tool. Micromachining forces, specific energies, effective coefficient of friction, shear angles, shear stresses, and chip morphology were examined for six crystallographic orientations at uncut chip thicknesses ranging from 5 μm to 20 μm and cutting speeds ranging from 5 mm/s to 15 mm/s. Three distinct types of forces were observed, including steady (Type-I), bistable (Type-II), and fluctuating (Type-III) force signatures. The forces were seen to vary by as much as threefold with crystallographic orientation. Although the effect of cutting speed was small, the uncut chip thickness was seen to have a significant orientation-dependent effect on average forces. Chip morphology, analyzed under scanning electron microscopy, showed shear-front lamella, the periodicity of which was seen to vary with crystallographic orientations and uncut chip thicknesses.
[DOI: 10.1115/1.2917268]

1 Introduction

As current trends toward miniaturization accelerate and more applications are realized, garnering a comprehensive understanding of the micromanufacturing processes becomes imperative for optimizing current technologies and developing future technologies. Mechanical micromachining, which includes the application of traditional machining techniques such as milling, drilling, and turning to the microscale, is gaining momentum as a flexible and efficient way to make truly three-dimensional microscale features and parts from a wide selection of materials [1–5]. Although kinematically similar, micromachining is fundamentally different from conventional (macro) machining.

An important difference arises from the considerable effect of workpiece microstructure on the micromachining processes [6–8]. Characteristic dimensions of grains in metals are commensurate with the uncut chip thickness values experienced in micromachining. Therefore, the process takes place within individual grains or within a few grains at a time. Since crystalline lattices exhibit elastic and plastic anisotropy [9], the mechanical properties change when crossing into different grains. Therefore, machining force magnitudes and direction, rake and flank-face friction, as well as amount of elastic recovery will vary during the process [7,8,10–20]. In contrast, since a large number of grains are encountered during macroscale cutting processes, an averaged effect from the workpiece microstructure is experienced, and the material can usually be assumed to behave isotropically.

Although there have been numerous studies on different aspects of cutting processes over the years, only a handful of those investigated micromachining of single-crystal materials. The first known study on single-crystal machining was published in 1950 by Clarebrough and Ogilivie [21], who microtomed large crystals of lead, and observed a strong correlation between the crystallographic orientation and lamellae spacing. Early studies of Black and co-workers shed light on various aspects of microscale chip formation in single-crystal cutting [15,22–24]. They performed a quantitative study of chip formation mechanisms in single-crystal copper and aluminum via an ultramicrotomy process with speeds of 1 mm/s and uncut chip thicknesses from 25 nm to 2 μm. Scanning electron microscopy (SEM) was used for the first time to examine chip morphology. It was hypothesized that the single-crystal cutting process involves a periodic chip-formation behavior referred to as shear-front lamella [23–25]. The compression ahead of the tool produces a dislocation cell structure. During shearing, this cell structure acts as a barrier, and the dislocations initiated from the tool tip must recombine to penetrate or circumvent this barrier. When the applied stress (from the tool) becomes sufficiently large, a catastrophic shear front develops as a narrow band. Therefore, the chips generated through this process include a periodic lamellae structure separated by narrow bands of shear fronts. During the annihilation of these shear fronts, a large amount of heat releases and temporarily reduces the shear stress; accordingly, the shear stress was considered to include thermal and athermal components. The lamellae thickness was seen to be affected by the crystallographic orientation and uncut chip thickness (below 2 μm) [23,24,26]. It was also observed that the crystals go through little rotation during shearing. Since the energy required for recombining dislocations depends on the stacking fault energy (SFE), SFE was considered as an important parameter in cutting of single crystals, where the materials with high SFE requires less energy to move through the metastable dislocation cell structures [22]. It was postulated that the vicinity of the preferred slip system (i.e., (111) [110] directions for face-centered cubic (fcc) metals) to the shear direction was critical in determining the shear behavior and the thickness of lamellae.

Cohen [27] performed in situ cutting experiment for the first time inside an SEM on single-crystal and polycrystalline aluminum and copper while measuring the machining forces. These plunge-turning experiments included continuously changing crys-

[1]Corresponding author.

Contributed by Manufacturing Engineering Division of ASME for publication in the JOURNAL OF MANUFACTURING SCIENCE AND ENGINEERING. Manuscript received May 30, 2006; final manuscript received December 17, 2007; published online June 3, 2008. Review conducted by Professor Shreyes N. Melkote.

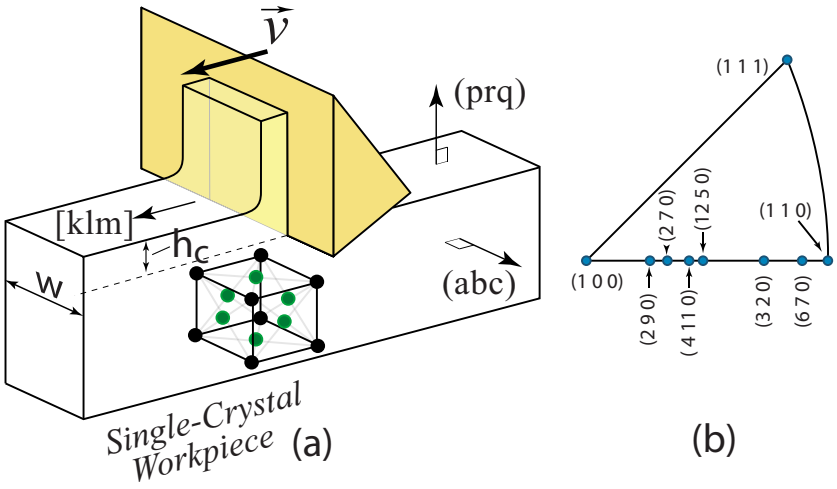

Fig. 1 (*a*) Diagram of the single-crystal cutting process and (*b*) projection of the crystallographic orientations onto the standard stereographic triangle

tallographic orientations. It was observed that the changes in cutting forces and shear angle exhibited a four-fold symmetry expected from the crystal structure of fcc metals. Contrary to the preceding literature, Cohen found that the shear stress varies with the crystallographic orientation and tool geometry. A simplified model for the shear angle was derived by minimizing the total energy expended for primary shear and rake-face friction [27].

Ueda et al. [13] presented an experimental study on orthogonal cutting of single-crystal β-brass inside an SEM. These *in-situ* observations of chip formation revealed significant variations in chip-formation mechanism at different crystallographic orientations. Sato et al. [28] presented an experimental investigation on orthogonal cutting of a textured material by turning the end of a tube made from a rolled aluminum sheet. The specific cutting energy and calculated shear angle were seen to periodically fluctuate during the process. They concluded that the period of fluctuations roughly corresponds to the orientation of the crystallographic texture. These observations motivated investigation of orthogonal cutting of single-crystal aluminum at specific crystallographic orientations [29–31]. Different orientations of single-crystal aluminum were machined, and it was seen that the specific energy varies with crystallographic orientation.

Various other works have investigated diamond turning and fly-cutting of single-crystal copper [11,14,18,19,32–36] and single-crystal aluminum [17,37,38]. Some studies found a correlation between different crystallographic orientations and resulting surface roughness [17,36,39]. Moriwaki and co-workers [11,39,40] observed that for uncut chip thicknesses below 0.1 μm when micromachining already-machined surfaces, the shear angle, cutting force, and surface roughness were not affected by the crystallographic orientation. This was explained by considering the significant subsurface damage (dislocations) left from previous cutting passes.

Although a number of studies have been performed through the years, our fundamental understanding on single-crystal machining has not advanced since the aforementioned works of Black, von Turkovich, and Cohen. This paper presents a careful experimental investigation on microplaning of single-crystal aluminum in six different crystallographic orientations for varying cutting speeds and uncut chip thicknesses. A diamond tool is used to perform orthogonal cutting to minimize the effects from the cutting edge radius and to simplify the cutting geometry. Unlike other studies in literature, the long cutting lengths used in each crystallographic orientation enabled revealing different types of forces and chip morphology that were not previously observed. Furthermore, the shear stresses and coefficients of friction were seen to vary not only with the crystallographic orientation, but also with the cutting conditions. Therefore, the presented experimental study furthers the fundamental understanding on the effect of crystallographic orientations in cutting forces, chip morphology, shear stress, and effective coefficient of friction for machining single-crystal aluminum.

2 Experimental Setup and Procedure

The experimental investigation presented here utilized a single-crystal diamond tool with a 2 mm straight cutting edge. The motivation behind using a sharp-edged diamond tool was to isolate the crystallographic effects of the workpiece by minimizing the complexities arising from the edge radius [41,42]. The tool provided a rake angle of 0 deg and a nominal clearance angle of 10 deg. To assess the edge sharpness and edge condition, atomic force microscope (AFM) measurements and SEM imaging of the diamond tool were conducted in a similar manner as in Ref. [42–45]. It was seen that the cutting edge has a few minor nicks with sizes less than 400 nm. By measuring multiple locations along the cutting edge, the average edge radius was determined to be 25.5 nm with a standard deviation of 9 nm. SEM imaging after the completion of the experiments indicated no measurable wear on the diamond tool.

2.1 Workpiece Characterization and Cutting Orientations. A schematic representation of the single-crystal microplaning process is given in Fig. 1(*a*). The cutting-plane normal, cutting direction, and the workpiece orientation (the width direction) are labeled using the Miller-index notation as (*prq*), [*klm*], and (*abc*), respectively. Also shown in the figure are the width of cut w, the uncut chip thickness h_c, and the cutting speed v.

The workpiece used in this work was a 99.999% pure single-crystal aluminum from Goodfellow Corp. with the (0 0 1) orientation (parallel to the axis of the workpiece). Originally, the workpiece was shaped as a disk with 2 mm thickness and 12 mm diameter. The thickness (width of cut) of the workpiece was reduced to 1 mm using the wire-electro discharge machining process, followed by a light polishing (using 0.1–1 μm aluminum-oxide abrasive particles) to remove the small damaged layer. The final width of cut was estimated to be 1 ± 0.020 mm. Laue X-ray diffraction measurements confirmed the single-crystalline nature and orientation of the workpiece.

Since aluminum is an fcc material, it exhibits cubic symmetry in its atomic lattice structure, and its mechanical behavior is strongly influenced by this symmetry [46]. When choosing the cutting planes, care was taken to distribute the crystalline orientation of these planes such that if symmetry is applied, the results

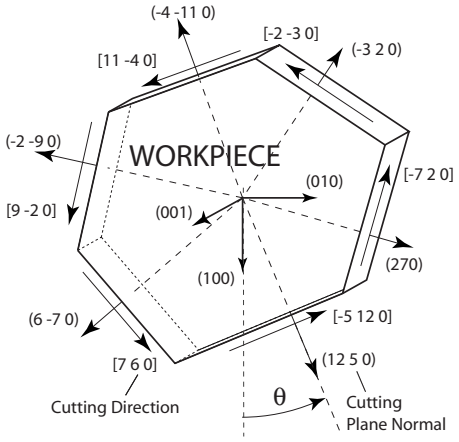

Fig. 2 Diagram of the cutting planes and cutting directions used during the experimentation

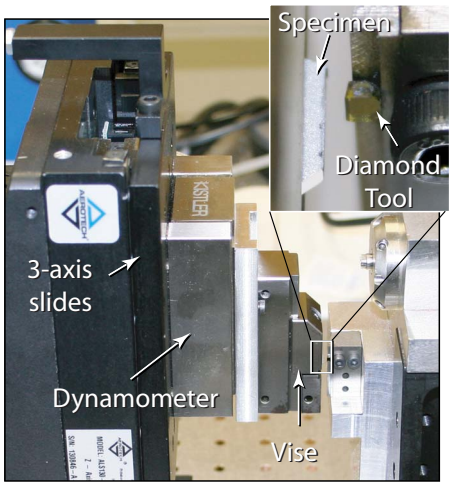

Fig. 3 The experimental testbed

can be extended to cover the entire range of crystallographic orientation about the [0 0 1] direction. Figure 1(*b*) shows the projection of the crystallographic orientations onto the standard stereographic base triangle for single-crystal aluminum and indicates the six cutting planes (facets) selected for the current investigation. Figure 2 depicts the workpiece and the crystallographic orientation of the facets with the normal and cutting directions on each facet. After the cutting experiments, Laue X-ray diffraction measurements were performed to determine the exact orientation of the cutting facets with 1 degree resolution.

A convenient way to represent the crystallographic orientations is to specify the angle of rotation of each plane normal from a specific direction. Table 1 provides the counterclockwise rotation (θ in Fig. 2) of each plane normal about the [0 0 1] direction from the [1 0 0] direction. Also given in Table 1 are the rotation γ of the cutting direction from (1 0 0) orientation, and the rotation α of the cutting plane normal from the (1 0 0) orientation when the crystallographic symmetry is considered. On the discussion below, the cutting facets are identified with the symmetric Miller-index notation (all positive numbers) of their normals or the (symmetric) rotation angles α.

2.2 Experimental Facility. The testbed used in this experimentation, shown in Fig. 3, is composed of a microplaning attachment integrated into a miniature machine tool platform with 10 nm resolution. A Phantom V7 camera enabled acquiring high-speed video images up to 160,000 frames/s with a 12× zoom lens. Three orthogonal machining-force components were measured with a Kistler 9256C1 MiniDyn dynamometer with a noise threshold less than 2 mN. The force data were collected with a minimum sampling rate of 1 kHz. The workpiece was held with a miniature vise, which was attached to the dynamometer.

A series of experiments were conducted to determine the loop stiffness of the experimental setup. A steel specimen with 10 $\times 10$ mm^2 cross section and 15 mm length was attached to the miniature vise in place of the workpiece. After contacting the tool fixture near the actual tool location, the slides were driven with a triangular wave with 3 μm amplitude. Actual deflection of both the slides and the tool fixture were measured using a laser Doppler vibrometer while simultaneously measuring the forces from the dynamometer. The captured forces and deflections showed a linear correlation. The loop stiffness of the system was calculated to be 1.7 N/μm in the direction normal to the cutting speed (i.e., the thrust direction). Further measurements indicated that the stiffness does not vary measurably along the cutting direction. During the experimentation, the *actual* uncut chip thickness h_c was determined for each case by subtracting the amount of deflection caused by the average (measured) thrust force from the *prescribed* uncut chip thickness h_{cp}.

Table 1 Miller indices and angular orientations of cutting facets and cutting directions

Cutting facet	θ (deg)	γ (deg)	α (deg)	$\Delta\theta$ (deg)
(–2 –9 0)	257.5	347.5	77.5	0.15
(2 7 0)	74.1	164.1	74.1	–0.69
(–4 –11 0)	200.0	290.0	20.0	0.08
(12 5 0)	22.6	112.6	22.6	0.27
(–3 2 0)	146.3	236.3	56.3	0.51
(6 –7 0)	310.6	40.6	40.6	0.21

3 Results and Discussion

The experiments were conducted at three cutting speeds (5 mm/s, 10 mm/s, and 15 mm/s) and three prescribed uncut chip thicknesses (5 μm, 10 μm, and 20 μm) on each of the six cutting facets of the workpiece. For each test case, at least three cuts were performed to ensure the repeatability of the results. Between each cut, multiple 1 μm depth cleanup cuts were performed to remove the material with possible subsurface damage from the previous cut. During the experiments, no stable built-up edge (BUE) was observed under any condition.

3.1 Characteristic Force Signatures. The forces experienced during this investigation can be categorized as one of the three distinct types (see Table 2). The force signature that is commonly seen during macroscale planing, where the forces rapidly rise and remain at a constant level until the end of the process, was seen in a number cases. This *steady* force signature is considered to be of Type-I, an example of which is given in Fig. 4(*a*). The Type-I force indicates a steady shearing/slip process associated with ei-

Table 2 The force types encountered under different speeds and depths (prescribed uncut chip thicknesses)

Speed v (mm/s)	5			10			15		
Depth h_{cp} (μm)	5	10	20	5	10	20	5	10	20
(2 9 0)	I	I	I	II	II	I	II	I	I
(2 7 0)	III	III	I	III	III	I	I	I	I
(4 11 0)	I	I	I	II	I	I	II	I	I
(12 5 0)	I	I	I	II	I	I	II	I	I
(3 2 0)	II	I	I	I	I	I	II	I	I
(6 7 0)	I	II	I	II	II	II	II	II	II

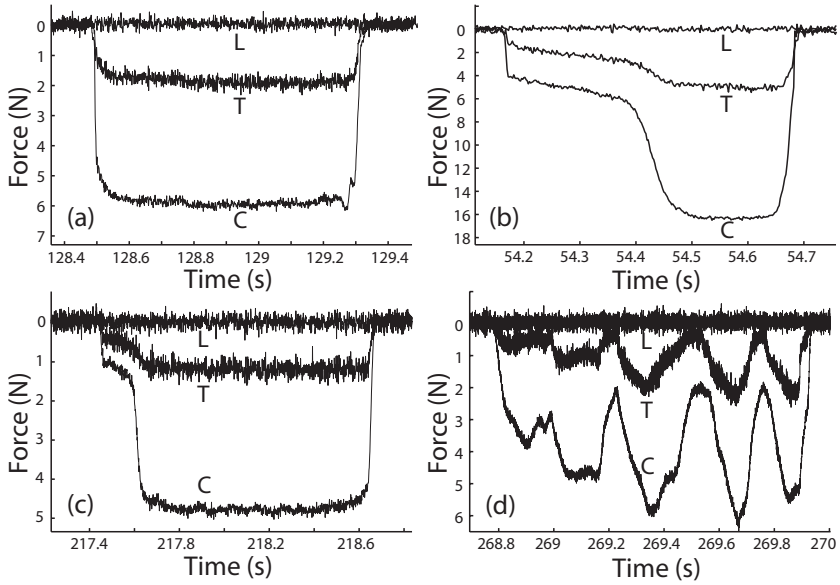

Fig. 4 Cutting (C), thrust (T), and lateral (L) forces for (*a*) (12 5 0) facet for 5 mm/s and 20 μm, (*b*) (6 7 0) facet with 10 mm/s and 20 μm, (*c*) (3 2 0) facet with 5 mm/s and 5 μm, and (*d*) (2 7 0) facet with 5 mm/s and 5 μm

ther single-slip behavior or persisting multislip behavior. High-speed video images collected during these conditions showed a steady chip-formation tendency, where the chip thickness and curvature remained unchanged throughout the cut.

A number of other cases produced a *bistable* force signature, in which two distinct force levels were experienced within a cut. Examples of this Type-II force signature are given in Figs. 4(*b*) and 4(*c*). Under different conditions, the behavior of Type-II forces was seen to vary considerably. The duration and relative magnitude of the two force levels strongly varied with crystallographic orientation and secondarily with cutting conditions. Generally speaking, increased uncut chip thickness seemed to delay the transition between the two force levels. Also, in most cases, the first portion of the forces was not constant, but rather showed a slow increase until reaching the transition point. The high-speed videos and SEM images of the chips indicated that the chip thickness and curvature drastically changed at the point of transition. Since the loop stiffness does not vary along the cutting direction, the Type-II behavior is not related to the stiffness.

The possible source of this behavior is the nonlinear bifurcations experienced in slip/shear behavior. It is possible that various strains are accumulating from the beginning of the cut, inducing increased strain hardening. When a certain level is reached, the state of the stress makes it energetically more preferable for slip to occur on a different system(s). This new slip system is also stable and it remains in effect until the end of the cut. This mechanism may also be assisted by the changes in friction (and secondary deformation) on the rake face since increased resistance to chip flow would favor activation of lower shear planes. It is postulated here that such a bistable phenomenon may not be observed when a large number of crystals are involved in cutting (macromachining), since the material behaves quasi-isotropically with average mechanical properties. This observation also suggests that for processes with interrupted chip formation (e.g., micromilling), the forces encountered for some crystallographic orientations would be lower than those for processes with continuous chip formation.

Another type of force signature observed during the tests is referred to as Type-III forces. The Type-III forces were characterized by large, cyclic fluctuations, such as those seen in Fig. 4(*d*). Only the forces in facet (2 7 0) indicated Type-III behavior. The variations of cutting and thrust forces reached 50% and 90% about the average values, respectively, when cutting with 5 μm prescribed uncut chip thickness and 5 mm/s speed. The severity of fluctuations decreased with increasing uncut chip thickness.

Various possible causes of these fluctuations include external vibrations, presence of unstable BUE, the loop stiffness of the setup, and periodic changes to the effective material characteristics. Since such fluctuations were not observed on other crystallographic orientations under the same cutting conditions when the force magnitudes were similar or higher, external (and self-excited) vibrations and loop stiffness can be ruled out as possible causes. Although the presence of an unstable BUE is a possible cause, absence of such fluctuations in other facets reduces its probability as a cause. In addition, the high-speed video images and post-test observations of the tool did not show any indication of BUE. Therefore, we can conclude that the observed phenomenon is directly related to the shear/slip behavior of single crystals. It is possible that, similar to the Type-II behavior, more than one preferable slip system exists. Unlike in Type-II, however, neither of the two slip systems possesses long-term stability. With changing stress state, the preferable slip system fluctuates between the two possible systems. Such force signatures are expected in symmetric orientations where two $\{111\}\ \langle 110\rangle$ slip systems are available.

3.2 Repeatability. To ensure the repeatability of the measurements, each test was repeated at least three times. Three repetitions of Type-III forces from facet (2 7 0) with 5 mm/s and 5 μm, for instance, are presented in Fig. 5; the high level of repeatability is clear even when severe fluctuations occur.

An analysis of variance (ANOVA) study was performed to assess the repeatability of the experiments using the average specific cutting energy values as the response metrics. All repetitions with three-level variations of cutting speed and uncut chip thickness were considered. The calculated values of an F-distribution are given in Table 3, where the statistically significant effects based on 95% confidence bands are given in bold. It is seen that, other than three instances, all the main effects were statistically significant. It can be concluded that the experiments captured the effects due to change in parameters since the variations between repetitions were much less than those between different sets of input

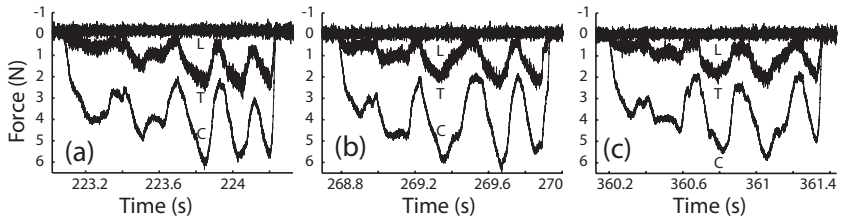

Fig. 5 Forces from three repetitions on (2 7 0) facet for 5 mm/s speed and 5 μm prescribed uncut chip thickness

parameters. This indicates the high level of repeatability of the experiments, as well as the suitability of experiments in investigating the effects of the considered parameters.

3.3 Specific Energies. Specific energies in cutting (normal) and thrust (friction) directions were calculated by dividing the average cutting and thrust forces, respectively, by the chip area. Figure 6 gives the cutting and thrust specific energies as a function of the actual uncut chip thickness h_c. In the case of Type-II forces, the averages from the first stable region were used to calculate the specific energies.

Table 3 *F*-values from the ANOVA analysis for specific cutting energies

Cutting facet	h_c	v	Interaction
(2 9 0)	1.15	**9.19**	**3.29**
(2 7 0)	**15.06**	**25.59**	**7.7**
(4 11 0)	**21.54**	0.29	0.36
(12 5 0)	**13.91**	**5.49**	**3.73**
(3 2 0)	**11.02**	3.1	0.27
(6 7 0)	**61.96**	**5.3**	**6.94**

Figure 6 shows the strong effect of the crystallographic orientation on specific energy. Generally, the lowest specific energies are experienced in the (6 7 0) facet. The highest specific cutting energies are seen in the (3 2 0) facet, reaching more than three times those in the (6 7 0) facet. Variations in specific thrust energy due to crystallographic orientations were seen to be less severe than those in specific cutting energy.

The well-known size effect is clearly seen in Fig. 6. The change in specific energies with uncut chip thickness is nearly uniform at different crystallographic orientations. Since a sufficiently sharp edge radius is utilized, those contributors to the size effect arising from the edge radius are less effective. Therefore, the main causes of the size effect in this case are material-related phenomena. In particular, deformations emanating from the tool tip affect a volume that is related nonlinearly to the uncut chip thickness. The size effect was seen to be less sensitive to the changes in cutting speed. Most importantly, the uniformity of the shift at different orientations indicates that the size effect phenomena in this case were independent of crystallographic orientations.

In addition to the conclusions reached above from Fig. 6, the effects of the cutting speed and uncut chip thickness can be as-

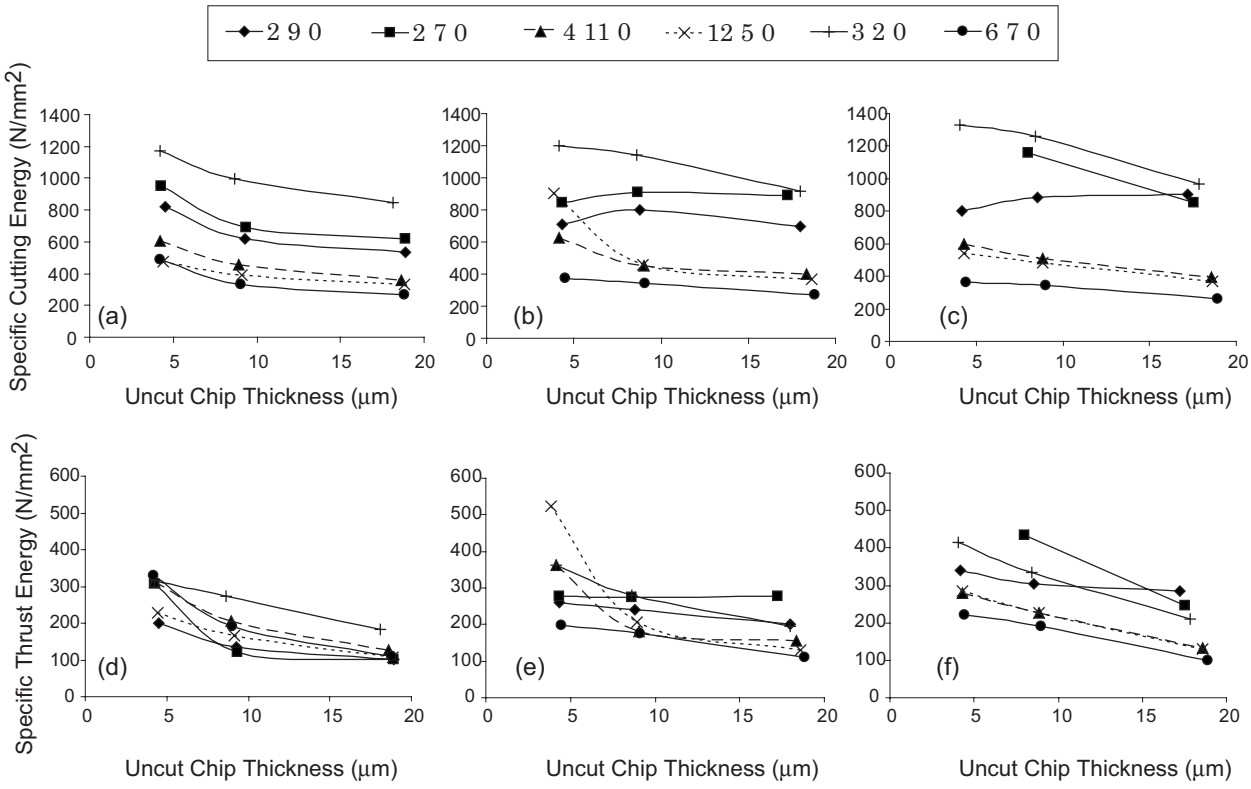

Fig. 6 The specific cutting energies for (*a*) 5 mm/s, (*b*) 10 mm/s, and (*c*) 15 mm/s; and the specific thrust energies for (*d*) 5 mm/s, (*e*) 10 mm/s, and (*f*) 15 mm/s

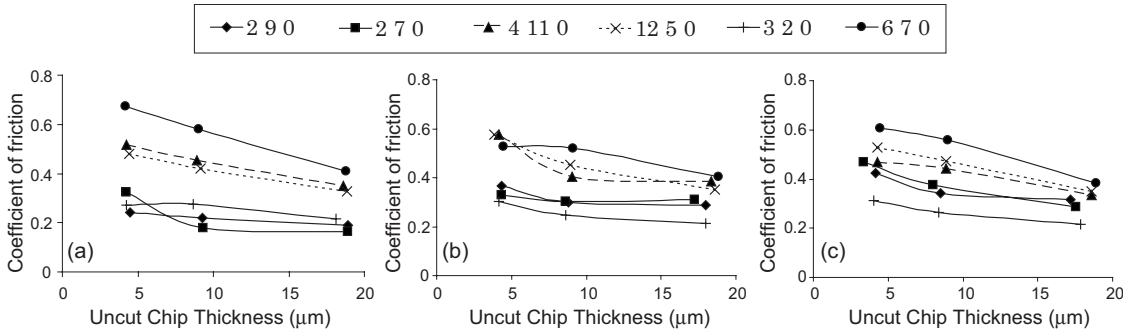

Fig. 7 The effective coefficient of friction for (*a*) 5 mm/s, (*b*) 10 mm/s, and (*c*) 15 mm/s

sessed referring to the ANOVA analysis given in Table 3. It is seen that other than in (2 9 0) and (2 7 0) orientations, the effect of uncut chip thickness is significantly larger than that of the cutting speed. When speed is statistically significant, the specific energies were seen to increase with increasing speed. This is expected since in microcutting the dominant effect of speed is related to the strain-rate effect (in contrast to thermal softening in macrocutting). The cutting speed was seen to have a stronger effect at small uncut chip thicknesses. It was also seen that (4 11 0) and (3 2 0) orientations were insensitive to the changes in cutting speed. On the other hand, (2 7 0) orientation, where the forces are of Type-III, showed a high level of sensitivity to cutting speed.

3.4 Coefficient of Friction. The ratio of specific thrust energy to specific cutting energy indicates the distribution of machining energy [27]. In the case of orthogonal cutting with zero rake angle, this ratio is equal to the effective coefficient of friction on the rake face. Figure 7 gives the effective coefficient of friction for constant levels of cutting speed. It is observed that the effective coefficient of friction shows significant variation with crystallographic orientation. Similar to the observations of Cohen [27], the orientation that produced the lowest specific cutting energies ((6 7 0) orientation) showed the highest proportion of energy expended to friction (and secondary deformation); and the orientation that produced the highest specific cutting energy ((3 2 0) orientation) showed the lowest proportion of energy to friction. These conclusions highlight the importance of friction and secondary deformation on the rake face in determining the characteristics of single-crystal material removal.

In general, lower chip thicknesses produced higher effective coefficients of friction. The effect of chip thickness on the effective coefficient of friction was seen to be almost uniform across the crystallographic orientations. Comparing Figs. 7(*a*)–7(*c*), it can be concluded that the cutting speed has less effect on the specific energy ratio.

3.5 Shear Angle and Shear Stress. According to Black [22], the shearing in single-crystal machining occurs along a thin shear zone [22]. In an orthogonal cutting process with the thin shear plane assumption, the shear angle ϕ can be calculated from the geometry of the cutting process and the chip ratio [47]. In this work, cut chip thicknesses were measured from SEM images. The calculated shear angles are given in Fig. 8. For few cases, the

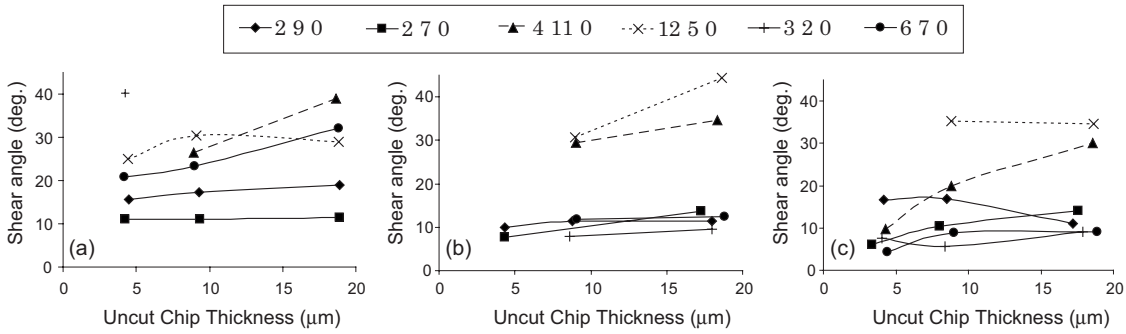

Fig. 8 Shear angles for (*a*) 5 mm/s, (*b*) 10 mm/s, and (*c*) 15 mm/s.

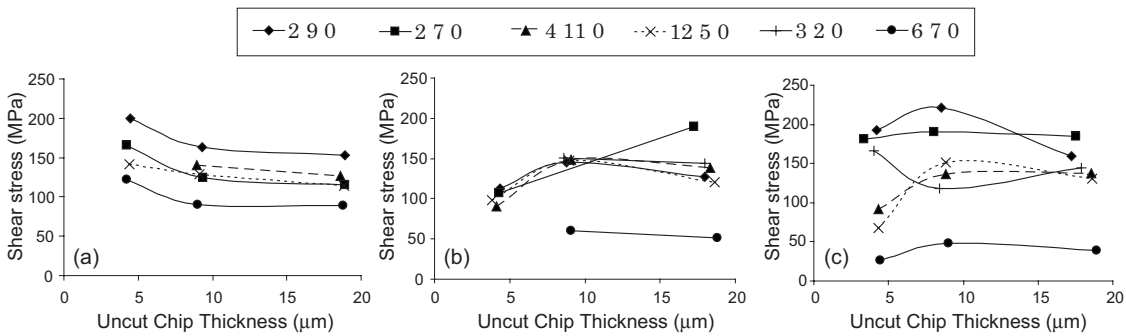

Fig. 9 Shear stresses for (*a*) 5 mm/s, (*b*) 10 mm/s, and (*c*) 15 mm/s

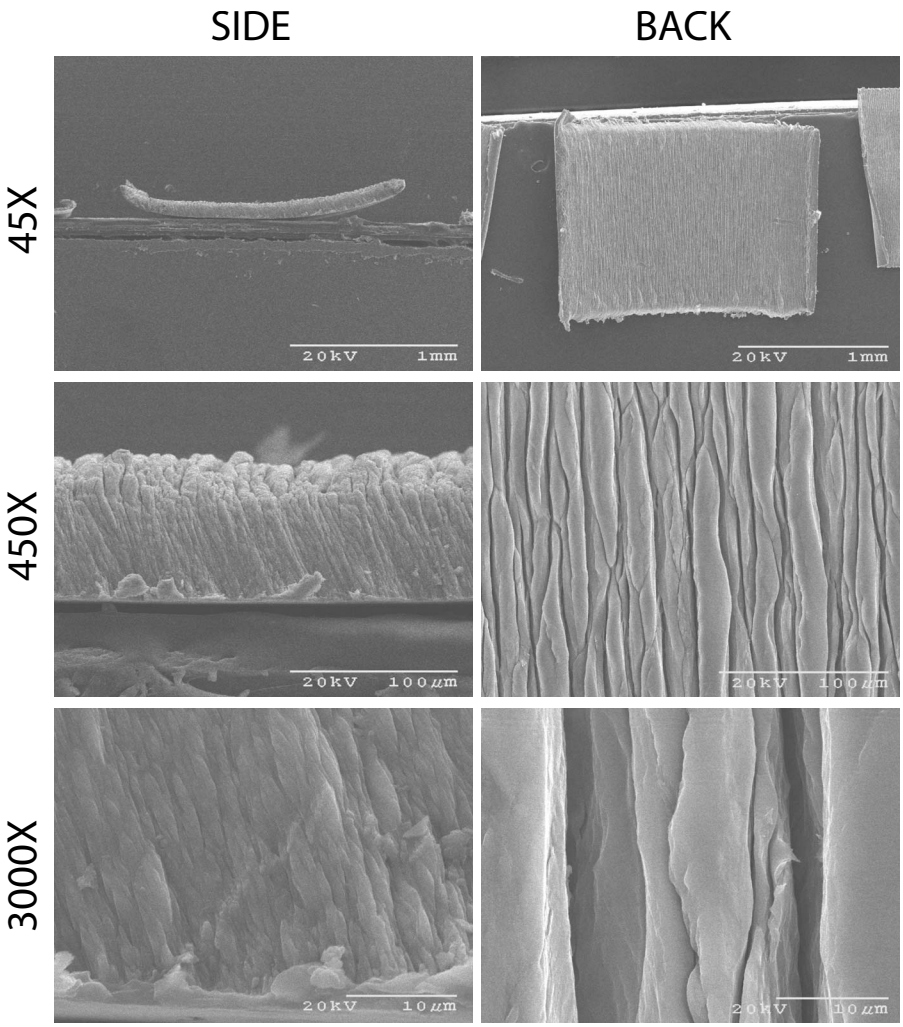

Fig. 10 SEM images of chips from the (2 7 0) orientation illustrating the perspectives and magnifications used in analysis

highly curled chips did not allow accurate measurement of cut chip thicknesses, and those cases were omitted from Fig. 8.

From Fig. 8, it is seen that the crystallographic orientation has a significant effect on shear angle. In most cases, the shear angle was not sensitive to the changes in uncut chip thickness. Comparing Figs. 8(*a*)–8(*c*), it can be concluded that cutting speed has a significant effect in determining the shear angle.

Using the calculated shear angles and average forces, effective shear stresses were then calculated. Figure 9 gives the effective shear stress values. The large variation (from 25 MPa in (6 7 0) at 5 μm prescribed uncut chip thickness and 15 mm/s cutting speed, to 450 MPa (not shown in Fig. 9) for (3 2 0) with 5 μm prescribed uncut chip thickness and 5 mm/s cutting speed) of shear stress with crystallographic orientations is striking. As expected, the lowest shear stress was seen in the (6 7 0) facet, which produced the lowest specific energy. This conclusion indicates that the shear stress is not constant; it varies strongly with the crystallographic orientations, and secondarily with the cutting conditions.

3.6 Chip Morphology. The morphology of the chips contain important information about the mechanics of the cutting process. To analyze the chip morphology for microplaning single-crystal aluminum, images of the chips were taken using an SEM with 45×, 450×, and 3000× magnifications. Due to chip collection and placement difficulty, images were not gathered for some of the cases. Both the profile and the back (the face of the chip that does not contact the rake face) of the chips were imaged.

Figure 10 gives the samples of the collected chip images. Chips were continuous in all cases. Moderate to high in-plane chip curl, where the axis of the curl was aligned with the width direction, was observed for most cases. Although the front sides of the chips were smooth, judging from the thickness (generally, well below 1 μm) of the deformed region on the front of the chips, the secondary shear was very small.

Measurable out-of-plane chip curl was not observed in any of the experiments. In addition, the closeness of the cut-chip width to uncut chip width suggested that the side spread was negligible. These observations indicate that the shear/slip process occurred in a plane perpendicular to (0 0 1) orientation. In other words, the process was effectively a plain-strain process.

The images of the back of chips such as Fig. 11 showed the shear-front lamella structure. For all of the crystallographic orientations, except for the (12 5 0) facet, increasing uncut chip thickness produced thicker lamellae, and the lamellae thickness was less sensitive to cutting speed. This is in agreement with Black's theory [23–25], which postulates that the deformation in a cutting process proceeds by conventional dislocation motion until strain hardening from dislocation locks reaches a critical point, at which time "catastrophic shear" occurs due to the thermal release from dislocation annihilation. This implies that the larger uncut chip thickness allows more dislocation motion before catastrophic shear, and thus results in the thicker lamellae. In other words, the

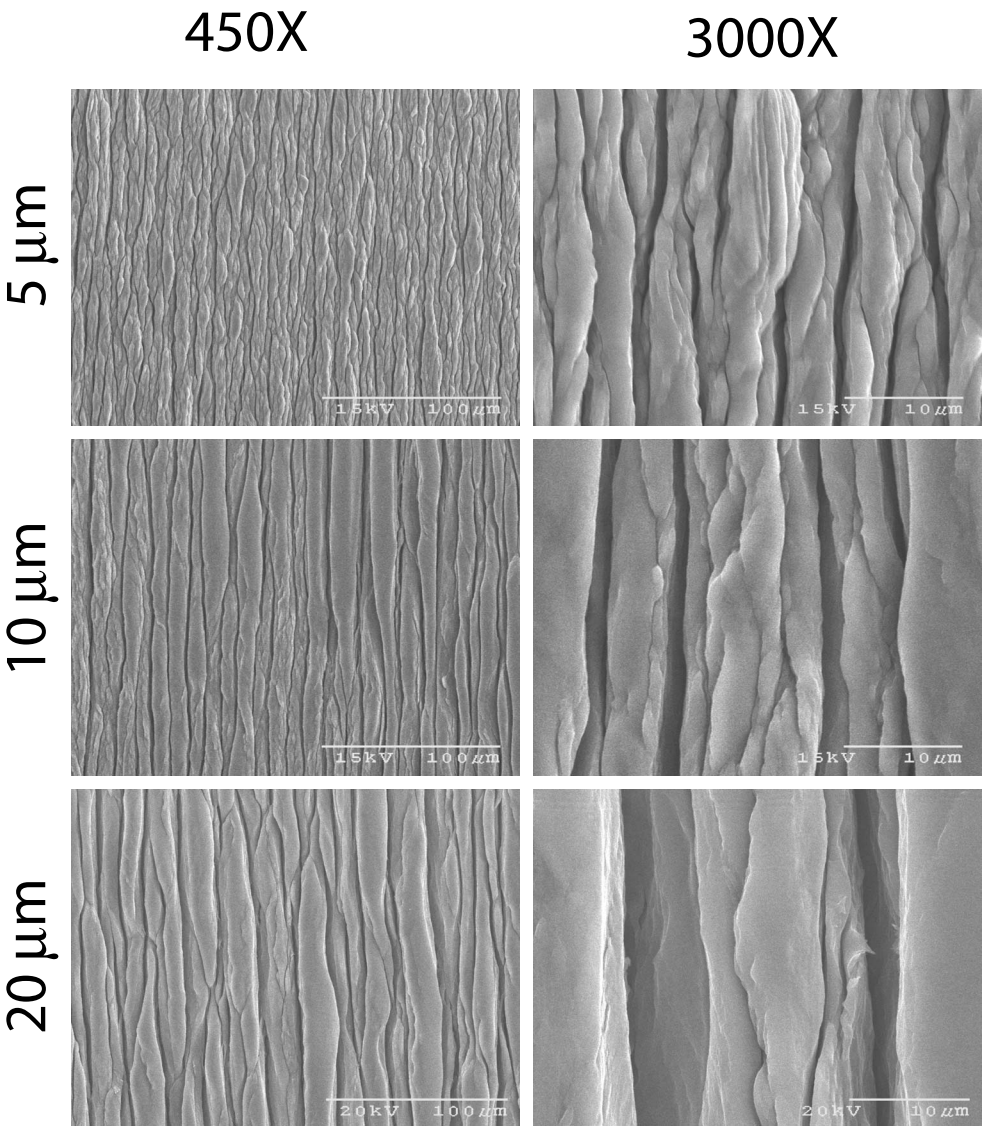

Fig. 11 SEM image of the face of the chips produced on the (2 7 0) orientation

time to reach the work hardening limit of the material is longer for larger uncut chip thicknesses. However, while Black observed the increase with lamellae thickness only up to 2 μm uncut chip thickness, in this work the lamellae thickness was seen to increase with uncut chip thickness up to 20 μm prescribed uncut chip thickness. Black [24,25] also stated that the lamellae thickness is not affected by the cutting speed because the dislocation motion is far faster than the cutting speed. Figure 11 shows the increase in the spacing of the lamellae for the (2 7 0) facet at 5 μm, 10 μm, and 20 μm prescribed uncut chip thicknesses and 15 mm/s cutting speed. The lamellae spacing increased by over 100% from approximately 8 μm to 17 μm. For the (12 5 0) facet, which produced mostly Type-I forces, the thickness of the lamellae was insensitive to the changes in uncut chip thickness. Figure 12 shows the chips for six crystallographic orientations for constant prescribed uncut chip thickness of 20 μm and speed of 15 mm/s. This figure indicates the strong effect of crystallographic orientation in lamellae spacing.

From the profile view of the chips, it was seen that the lamellae changed character through the thickness of the chip; the lamellae were thinner toward the front of the chip, where it contacted the rake face. This phenomenon was most visible for the (2 9 0) orientation. Figure 13 shows the difference between the appearance of the lamellae thickness from the back and the profile of the chip for the (2 9 0) orientation at 10 mm/s and 20 μm prescribed uncut chip thickness, where the lamellae appear thinner closer to the front of the chip than to the back of the chip.

The cut-chip thicknesses reflected the force variations experienced for the cases where Type-II or Type-III forces were encountered. Figure 14 illustrates the cut chip thicknesses and lamellae from the (6 7 0) facet with 10 mm/s cutting speed and 20 μm prescribed uncut chip thickness before and after the transition. It is clear that the chip thickness and lamellae thickness significantly increased after the transition point for this bistable case. The lamellae thickness as measured from the back of the chip varied from less than 1 μm to greater than 4 μm, and cut-chip thickness varied from approximately 33 μm to 117 μm, an increase of over 350%. It should be noted that, for this case, the mean force increased from 4.90 N and 16.13 N (over 325%) through the transition. The largest change in cut-chip thickness (from 5 μm to 45 μm, a change of 900%) was seen on the (6 7 0) facet with 5 μm prescribed uncut chip thickness and 15 mm/s cutting speed. Cyclic chip thickness variations were observed for the (2 7 0) facet associated with the Type-III forces. Those data were cor-

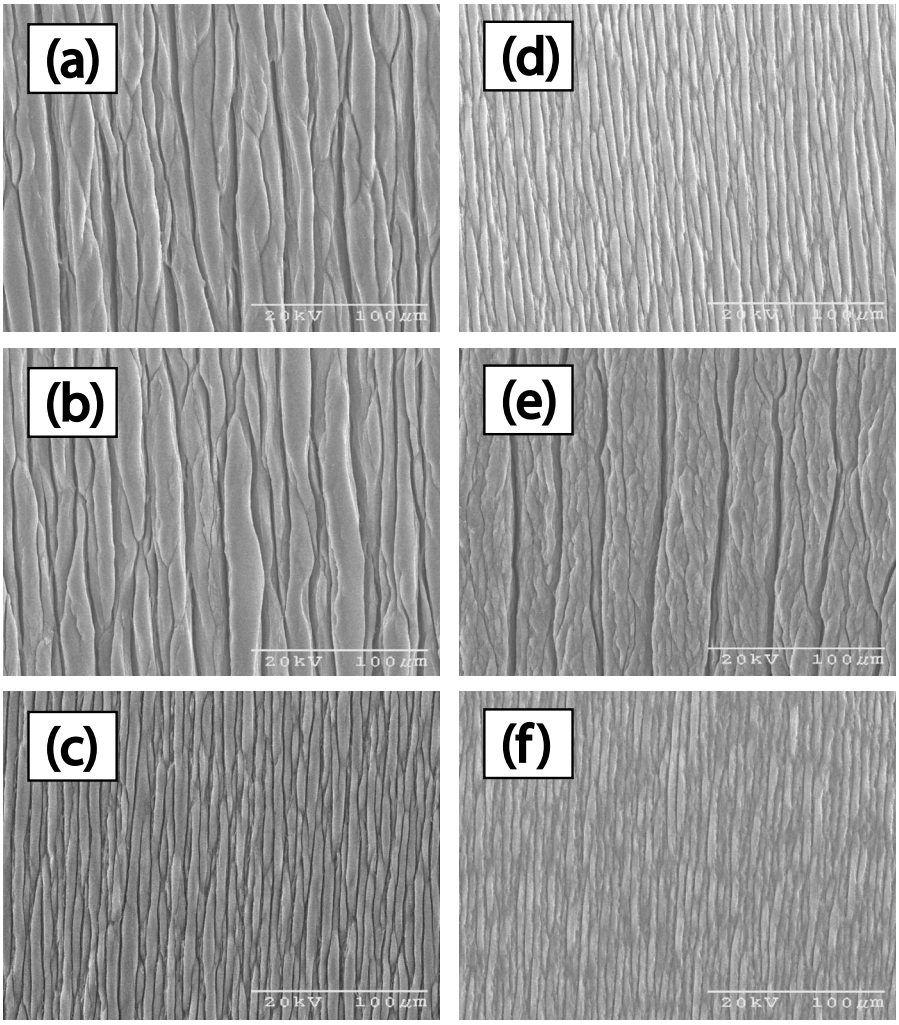

Fig. 12 Shear-front lamella at 20 μm prescribed uncut chip thickness and 15 mm/s speed for (*a*) (2 9 0), (*b*) (2 7 0), (*c*) (4 11 0), (*d*) (12 5 0), (*e*) (3 2 0), and (*f*) (6 7 0) crystallographic orientations

roborated with the high-speed video images, where Type-II and Type-III cases produced visible changes to chip curvature at times corresponding to force variations.

These observations indicate that a fundamental change in the chip-formation process occurred during the transition for the cases with Type-II forces, and the force fluctuations were reflected in cut-chip thicknesses for the cases with Type-III forces.

4 Summary and Conclusions

This paper presented an experimental investigation on orthogonal cutting of single-crystal aluminum using a diamond tool. Uncut chip thicknesses and cutting speeds were varied while cutting six different crystallographic orientations of the workpiece. Cutting forces, chip morphology, shear stresses, shear angle, and ef-

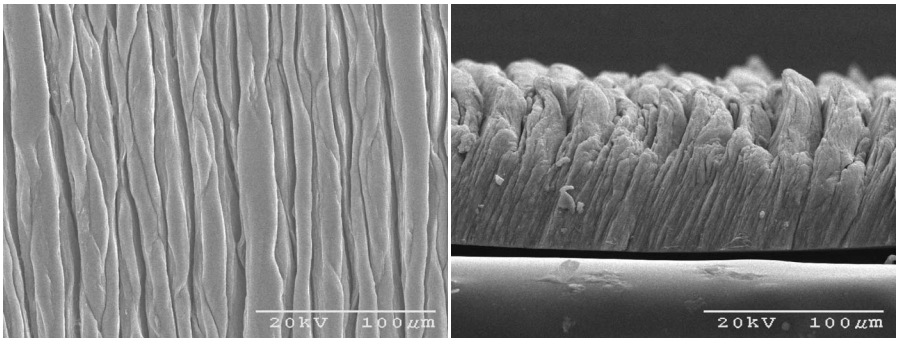

Fig. 13 450× magnification SEM image illustrating the difference between the apparent thickness of the lamella from the face and the profile views for the (2 9 0) orientation at 10 mm/s and 20 μm prescribed uncut chip thickness

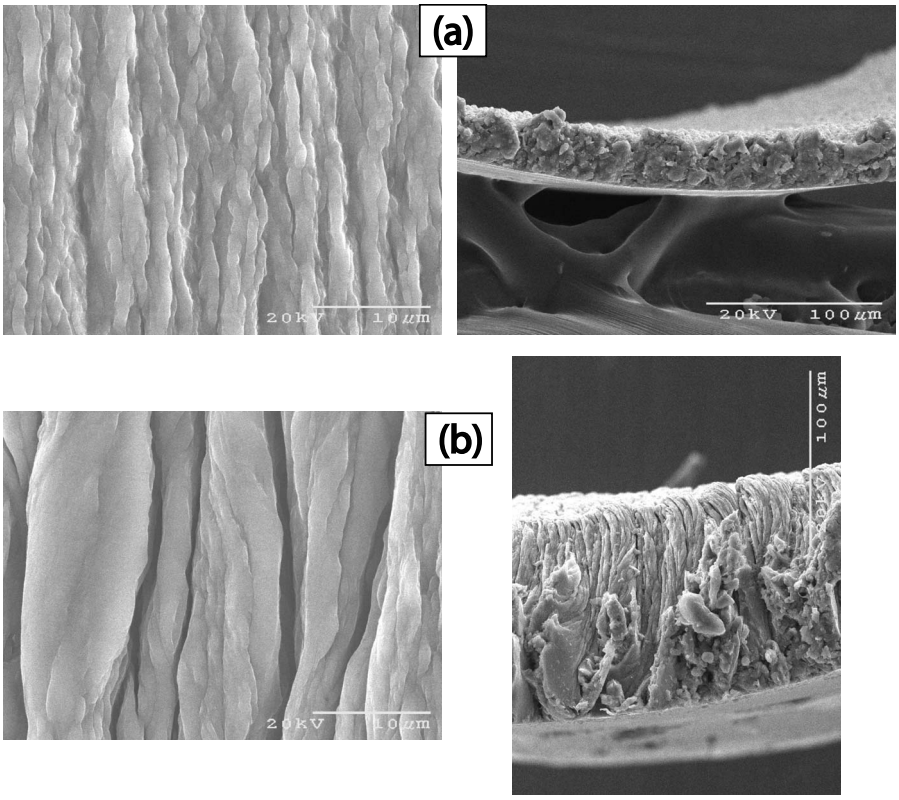

Fig. 14 SEM image comparing lamellae and chip thicknesses before (top) and after (bottom) the transition for the bistable case of the (6 7 0) orientation with v=10 mm/s and h_{cp}=20 μm

fective coefficient of friction were carefully analyzed for each experiment. The repeatability of the experimentation was shown through an ANOVA analysis. The following specific conclusions have been drawn from the presented work:

- Three distinct types of force signatures, including steady (Type-I), bistable (Type-II), and fluctuating (Type-III) forces are encountered when cutting single-crystal aluminum at different orientations. The bistable force can be observed only if the cutting length at a given crystallographic orientation is sufficiently long. The causes of the observed bistable and fluctuating force signatures are the unsteady slip behavior of the single crystals and the changes in frictional characteristics on the rake face.
- Specific energies vary by as much as threefold in different orientations. The highest and the lowest specific energies are seen when cutting the (3 2 0) and (6 7 0) facets, respectively. The specific energies significantly vary with uncut chip thickness, whereas the variation with cutting speed is small. The size effect is independent of crystallographic orientations.
- The lowest effective coefficient of friction, and thus the lowest amount of energy expended for friction as compared to shearing, is on the orientation with the highest specific cutting energy ((3 2 0) orientation), and vice versa. The effective coefficient of friction varies with crystallographic orientations and uncut chip thickness.
- Both the shear angle and shear stress depend considerably on the crystallographic orientations, but they are less sensitive to changes in cutting conditions. A significant variation in shear stress (from 25 MPa to 450 MPa) was seen at different crystallographic orientations. The orientation with the lowest shear stress ((6 7 0) orientation) coincides with that with the lowest specific cutting energy.
- The shear-front lamella is observed as the basic chip structure. The lamellae spacing significantly changes with crystallographic orientation. The lamellae spacing increases with increasing uncut chip thickness, including uncut chip thickness values higher than 2 μm [22]. The lamellae spacings are not sensitive to the changes in cutting speed. The behaviors of three distinct force types are reflected in the cut chip thicknesses.

Acknowledgment

The authors would like to thank Sara Rockwell for her help in analyzing the data, and Matt Wasserman, Luke Xie, Alex Long, and Caroline Conley for their assistance during testing and experimental analysis. The authors would like to acknowledge UPMC bioimaging laboratory for the use of its SEM. The discussions with Professors A. D. Rollett and A. Acharya were appreciated. The authors would also like to acknowledge Aerotech, Inc. for its generous contributions. This work was supported partly by the MRSEC program of the National Science Foundation under Award No. DMR-0520425, and by the NSF CAREER program under Award No. DMI-0547534.

References

[1] Benavides, G. L., Adams, D. P., and Yang, P., 2001, "Meso-Machining Capabilities," Technical Report No. SAND2001-1708, Sandia National Laboratories, Albuquerque, NM.
[2] Ehmann, K. F., Bourell, D., Culpepper, M. L., Hodgson, T. J., Kurfess, T. R., Madou, M., Rajurkar, K., and DeVor, R. E., 2005, *WTEC Panel Report on International Assessment of Research and Development in Micromanufacturing*, World Technology Evaluation Center (WTEC), Inc., Baltimore, MD.
[3] Liu, X., DeVor, R. E., Kapoor, S. G., and Ehmann, K. F., 2004, "The Mechanics of Machining at the Microscale: Assessment of the Current State of the Science," ASME J. Manuf. Sci. Eng., **126**, pp. 666–678.
[4] Filiz, S., Conley, C., Wasserman, M., and Ozdoganlar, O., 2007, "An Experimental Investigation of Micro-Machinability of Copper 101 Using Tungsten

Carbide Micro-Endmills," Int. J. Mach. Tools Manuf., **47**, pp. 1088–1100.
[5] Xie, L., Brownridge, S. D., Ozdoganlar, O. B., and Weiss, L. E., 2006, "The Viability of Micromilling for Manufacturing Mechanical Attachment Components for Medical Applications," Trans. NAMRI/SME, **34**, pp. 445–452.
[6] Kim, C.-J., Bono, M., and Ni, J., 2002, "Experimental Analysis of Chip Formation in Micro-Milling," Trans. NAMRI/SME, **30**, pp. 247–254.
[7] Vogler, M. P., DeVor, R. E., and Kapoor, S. G., 2004, "On the Modeling and Analysis of Machine Performance in Micro-Endmilling, Part I: Surface Generation," J. Manuf. Sci. Eng., **126**(4), pp. 685–694.
[8] Vogler, M. P., DeVor, R. E., and Kapoor, S. G., 2004, "On the Modeling and Analysis of Machine Performance in Micro-Endmilling, Part II: Cutting Force Prediction," J. Manuf. Sci. Eng., **126**(4), pp. 695–705.
[9] Dow, T. A., and Scattergood, R. O., 2003, "Mesoscale and Microscale Manufacturing Processes: Challenges for Materials, Fabrication and Metrology," Proceedings of the ASPE Winter Topical Meeting, Vol. 28, pp. 14–19.
[10] Spath, D., and Huntrup, V., 1999, "Micro-Milling of Steel for Mold Manufacturing—Influences of Material, Tools and Process Parameters," Precis. Eng., **1**, pp. 203–206.
[11] Moriwaki, T., and Okuda, K., 1989, "Machinability of Copper in Ultra-Precision Micro-Diamond Cutting," CIRP Ann., **38**(1), pp. 115–118.
[12] Eda, H., Kishi, K., and Ueno, H., 1987, "Diamond Machining Using a Prototype Ultra-Precision Lathe," Precis. Eng., **9**(3), pp. 115–122.
[13] Ueda, K., Iwata, K., and Nakajama, K., 1980, "Chip Formation Mechanism in Single Crystal Cutting β-Brass," CIRP Ann., **29**(1), pp. 41–46.
[14] Koenig, W., and Spenrath, N., 1991, "Influence of the Crystallographic Structure of the Substrate Material on Surface Quality and Cutting Forces in Micromachining," Proceedings of the International Precision Engineering Seminar, pp. 141–151.
[15] vonTurkovich, B., and Black, J. T., 1970, "Micro-Machining of Copper and Aluminum Crystals," ASME J. Eng. Ind., **92**, pp. 130–134.
[16] Ramalingam, S., and Black, J. T., 1972, "On the Metal Physical Considerations in the Machining of Metals," ASME J. Eng. Ind., **94**, pp. 1215–1224.
[17] To, S., Lee, W. B., and Chan, C. Y., 1997, "Ultraprecision Diamond Turning of Aluminum Single Crystals," J. Mater. Process. Technol., **63**, pp. 157–162.
[18] Yuan, Z. J., Lee, W. B., Yao, Y. X., and Zhou, M., 1994, "Effect of Crystallographic Orientation on Cutting Forces and Surface Quality in Diamond Cutting of Single Crystal," CIRP Ann., **43**(1), pp. 39–42.
[19] Zhou, M., Ngoi, B. K. A., Zhong, Z. W., and Wang, X. J., 2001, "The Effect of Material Microstructure on Microcutting Processes," Mater. Manuf. Processes, **16**, pp. 815–828.
[20] Vogler, M. P., DeVor, R. E., and Kapoor, S. G., 2003, "Microstructure-Level Force Prediction Model for Micro-Milling of Multi-Phase Materials," ASME J. Manuf. Sci. Eng., **125**, pp. 202–209.
[21] Clarebrough, L. M., and Ogilivie, G. J., 1950, *Microstructure by Machining, Machining Theory and Practice*, ASM, Metals Park, OH.
[22] Black, J. T., 1969, "Plastic Deformation in Ultramicrotomy of Copper and Aluminum," Ph.D. thesis, University of Illinois, Urbana, IL.
[23] Black, J. T., 1971, "On the Fundamental Mechanism of Large Strain Plastic Deformation," ASME J. Eng. Ind., **93**, pp. 507–526.
[24] Black, J., 1972, "Shear-Front-Lamella Structure in Large Strain Plastic Deformation Processes," ASME J. Eng. Ind., **94**, pp. 307–316.
[25] Black, J. T., 1979, "Flow Stress Model in Metal Cutting," ASME J. Eng. Ind., **101**, pp. 403–415.
[26] Blake, P. N., and Scattergood, R. O., 1986, "Chip Topography of Diamond Turned Ductile Metals," Proc. SPIE, **676**, pp. 96–103.
[27] Cohen, P. H., 1982, "The Orthogonal In-Situ Machining of Single and Polycrystalline Aluminum and Copper," Ph.D. thesis, Ohio State University, Columbus, OH.
[28] Sato, M., Kato, Y., and Tuchiya, K., 1978, "Effects of Material Anisotropy Upon the Cutting Mechanism," Trans. Jpn. Inst. Met., **19**, pp. 530–536.
[29] Sato, M., Kato, Y., and Tsutiya, K., 1979, "Effects of Crystal Orientation on the Flow Mechanism in Cutting Aluminum Single Crystal," Trans. Jpn. Inst. Met., **20**, pp. 414–422.
[30] Sato, M., Kato, Y., Tsutiya, K., and Aoki, S., 1981, "Effects of Crystal Orientation on the Cutting Mechanism of Aluminum Single Crystal," Bull. JSME, **24**, pp. 1864–1870.
[31] Sato, M., Kato, Y., Aoki, S., and Ikoma, A., 1983, "Effects of Crystal Orientation on the Cutting Mechanism of Aluminum Single Crystal," Bull. JSME, **26**(215), pp. 890–896.
[32] Wang, Z. Y., Sahay, C., and Rajurkar, K. P., 1994, "Micro-Turning of Copper With Monocrystal Diamond Tool," Proceedings of the First S.M. Wu Symposium on Manufacturing Science, Vol. 1, pp. 97–100.
[33] Zhou, M., and Ngoi, B. K. A., 2001, "Effect of Tool and Workpiece Anisotropy on Microcutting Processes," Proc. Inst. Mech. Eng., Part B, **215**, pp. 13–19.
[34] Moriwaki, T., Sugimura, N., Manabe, K., and Iwata, K., 1991, "A Study on Orthogonal Micro Machining of Single Crystal Copper," Trans. NAMRI/SME, **XIX**, pp. 177–182.
[35] Moriwaki, T., Okuda, K., and Shen, J. G., 1993, "Study on Ultraprecision Orthogonal Microdiamond Cutting of Single-Crystal Copper," JSME Int. J., Ser. C, **36**, pp. 400–406.
[36] Lee, W., To, S., and Cheung, C. F., 2000, "Effect of Crystallographic Orientation in Diamond Turning of Copper Single Crystals," Scr. Mater., **42**, pp. 937–945.
[37] Sato, M., Yamazaki, T., Shimizu, Y., and Takabayashi, T., 1991, "A Study on the Microcutting of Aluminum Single Crystals," JSME Int. J., Ser. III, **34**(4), pp. 540–545.
[38] Lee, W. B., Cheung, C. F., and To, S., 2003, "Friction-Induced Fluctuation of Cutting Forces in the Diamond Turning of Aluminum Single Crystals," Proc. Inst. Mech. Eng., Part B, **217**, pp. 615–631.
[39] Jasinevicius, R. G., Duduch, J. G., Porto, A. J. V., and Purquerio, B. M., 1999, "Critical Aspects on the Behavior of Material From the Mechanical Tool-Workpiece Interaction in Single Point Diamond Turning," J. Braz. Soc. Mech. Sci., **21**(3), pp. 509–518.
[40] Moriwaki, T., Sigimura, N., and Luan, S., 1993, "Combined Stress, Material Flow and Heat Analysis of Orthogonal Micromachining of Copper," CIRP Ann., **42**, pp. 75–78.
[41] Donaldson, R. R., Syn, C. K., and Taylor, J. S., 1987, "Minimum Thickness of Cut in Diamond Turning of Electroplated Copper," Second Annual ASPE Conference, Columbus, OH.
[42] Ikawa, N., Donaldson, R., Komanduri, R., Koenig, W., Aachen, T., McKeown, P., Moriwaki, T., and Stowers, I., 1991, "Ultraprecision Metal Cutting. The Past, the Present and the Future," CIRP Ann., **40**(2), pp. 587–594.
[43] Lucca, D. A., and Seo, Y. W., 1993, "Effect of Tool Edge Geometry on Energy Dissipation in Ultraprecision Machining," CIRP Ann., **42**(1), pp. 83–86.
[44] Drescher, J., 1993, "Scanning Electron Microscopic Technique for Imaging a Diamond Tool Edge," Precis. Eng., **15**(1), pp. 112–114.
[45] Evans, C., Polvani, R., Postek, M., and Rhorer, R., 1987, "Some Observations on Tool Sharpness and Sub-Surface Damage in Single Point Diamond Turning," Proc. SPIE, **802**, pp. 52–66.
[46] Kocks, U. F., Tome, C. N., and Wenk, H. R., 1998, *Texture and Anisotropy: Preferred Orientations in Polycrystals and Their Effect on Materials Properties*, Cambridge University Press, Cambridge.
[47] Merchant, M. E., 1945, "Mechanics of Metal Cutting Process. I. Orthogonal Cutting and a Type 2 Chip," J. Appl. Phys., **16**, pp. 267–275.